Chinese Chemical Letters 33 (2022) 4803–4807

Contents lists available at ScienceDirect

Chinese Chemical Letters

journal homepage: www.elsevier.com/locate/cclet

CDs assembled metal-organic framework: Exogenous coreactant-free biosensing platform with pore confinement-enhanced electrochemiluminescence

Xiu-Li Tao, Mei-Chen Pan, Xia Yang*, Ruo Yuan, Ying Zhuo*

Key Laboratory of Luminescence Analysis and Molecular Sensing (Southwest University), Ministry of Education, College of Chemistry and Chemical Engineering, Southwest University, Chongqing 400715, China

ARTICLE INFO

Article history:
Received 19 October 2021
Revised 23 November 2021
Accepted 5 January 2022
Available online 13 January 2022

Keywords:
Carbon dots
Zeolitic imidazolate framework-8
Pore confinement-enhanced ECL
Exogenous coreactant-free
Uric acid

ABSTRACT

Despite the various synthesis approachs to obtain luminous carbon dots (CDs), it is still quite challenging to construct the efficient electrochemiluminescence (ECL) owing to their low ECL reactivity and easy agglomeration. Herein, an efficient and concise ECL system was skillfully constructed by taking advantage of the nitrogen and sulfur co-doped CDs (N,S-CDs) with surfaces rich in hydrazide groups as luminophors to emit intense ECL, and metal-organic framework (MOF) as the matrix to confine CDs in its nanospace. Surprisingly, the proposed CDs assembled MOF (CDs/ZIF-8) enhanced anodic ECL signal up to 250% of pure CDs under the exogenous coreactant-free condition. As a proof of concept, the highly sensitive detection of uric acid (UA) was realized by the constructed ECL platform with a low detection limit of 3.52 nmol/L ranging from 10 nmol/L to 50 μmol/L. This work expanded ideas for the application of pore confinement effect, and provided references for the detection of disease biomarkers of gout and hyperuricemia.

Carbon dots (CDs) [1,2] have received increasing attentions with characteristics of unique biocompatibility, low cost and facile functionalization [3,4]. Nevertheless, the development of CDs in electroluminescence (ECL) biological analysis is limited due to the low ECL reactivity, weak signal intensity and easy agglomeration. Recently, the mentioned limitations have been addressed greatly through the strategies of hetero-atoms doping [5,6] and surface engineering to CDs [7,8]. For instance, Raju *et al.* [9] synthesized phosphorous doped carbon dots (P-CDs), which altered the electronic state levels to obtain a lower excitation potential. Arcudi and co-workers [10] improved the ECL emission intensity by modifying the amino groups on the surface of CDs. It can be seen that the dominant avenue is to focus on how to improve the properties of CDs themselves rather the ECL reaction microenvironment. Lately, an efficient pore confinement-enhanced ECL was reported by our group, which significantly increased the luminous efficiency of SnO_2 nanocrystal xerogel with hierarchically porous structure *via* the construction of confined reaction microenvironment [11]. Thus, it is extremely necessary to focus on the high luminescent efficiency and favorable reaction microenvironment of CDs for the construction of high performance solid-state ECL biosensors.

Despite the ECL binary system consisted of the luminophor and coreactant has excellent ECL intensity and efficiency, the addition of exogenous coreactants, such as hydrogen paroxide (H_2O_2), tri-*n*-propylamine (TPrA) and peroxydisulfate ($S_2O_8^{2-}$), suffers from toxicity and poor stability in aqueous solutions [12–14]. Unlike classical exogenous coreactants, dissolved O_2 exhibits distinctive advantages, including biocompatibility, low toxicity and without involving any extra addition, making it as an extremely promising coreactant. Nevertheless, its low reactivity for reactive oxygen species (ROSs) generation has been the notable drawback in its biosensing application [15]. Therefore, it is a critical step to increase the production of the ROSs from dissolved O_2 in the construction of exogenous coreactant-free biosensing platform. In our previous work, covalent organic frameworks (COF) could be used as ECL microreactors [16] to achieve significantly enhanced ECL in tris(2,2′-bipyridyl) ruthenium(II)/TPrA system ($Ru(bpy)_3^{2+}$/TPrA), because the TPrA as exogenous coreactant could be *in situ* readily reduced to the active $TPrA^{\bullet}$ in the porous nanochannels of COF by means of the pore confinement effect [11]. Recently, with the in-depth researches on organic frameworks materials, metal-organic frameworks (MOF) [17,18] with highly ordered channels assembled by metal ions and organic/inorganic ligands has shown a spectacularly catalytic effect on dissolved O_2 efficiently. For instance, zeolitic

* Corresponding authors.
E-mail addresses: xiayang2@swu.edu.cn (X. Yang), yingzhuo@swu.edu.cn (Y. Zhuo).

https://doi.org/10.1016/j.cclet.2022.01.010
1001-8417/

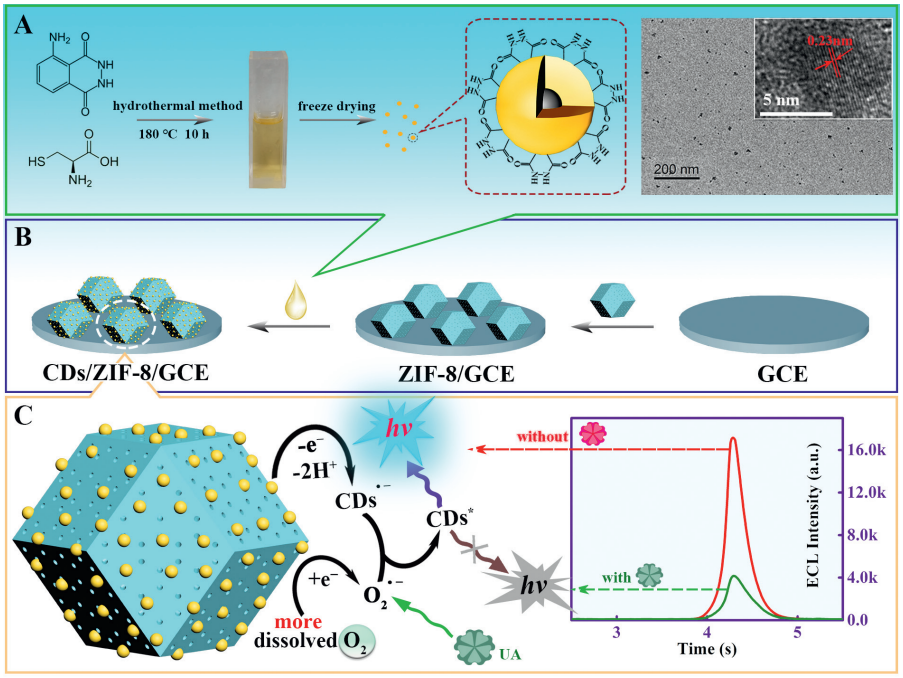

Scheme 1. Schematic representation of (A) the preparation of CDs, (B) the modification process of sensing electrode (CDs/ZIF-8/GCE) and (C) the possible ECL mechanism of CDs/ZIF-8/GCE for UA detection.

imidazolate framework-8 (ZIF-8), as a rhombic dodecahedron MOF, was demonstrated that it met the prerequisite for efficient catalytic reduction of dissolved O_2 for its abundant pyridine nitrogen (C—N bond) [19]. Inspired by this, we inferred that ZIF-8 could emerge as a promising candidate in constructing exogenous coreactant-free biosensor platform owing to the increased production of the ROSs. Herein, ZIF-8 could not only provide the confined spaces to preconcentrate dissolved O_2 for the pore confinement effect, but also had a significant effect on catalytic reduction of dissolved O_2 for the existence of abundant C—N bond. To sum up, ZIF-8 furnished a favorable matrix for building efficient and concise CDs based-ECL biosensors.

In this work, through the combination of pre-placement strategy to CDs and "pore confinement-enhanced ECL" effect, an efficient and concise ECL system based on CDs assembled ZIF-8 had been constructed skillfully, which decreased excitation potential effectively, and enhanced notably the luminescence intensity and stability of CDs (Scheme 1). Firstly, the CDs were prepared with the hydrothermal synthesis by using luminol to provide abundant hydrazide modified surface groups, L-cysteine to supply N and S doping sources, achieving low excitation potential and high ECL intensity (Scheme 1A). Then, the CDs were assembled into ZIF-8 *via* π-π stacking and hydrogen bonding as driving forces, which increased the immobilization amount and stability of CDs (Scheme 1B). More importantly, ZIF-8 could preconcentrate dissolved O_2 through the porous structure and promote the productivity of ROSs in virtue of the abundant existence of pyridine nitrogen in framework, achieving the construction of the efficient and concise CDs-based exogenous coreactant-free ECL biosensors. As a proof of concept, the constructed ECL platform was highly sensitive for the detection of uric acid (UA) with a low detection limit of 3.52 nmol/L ranging from 10 nmol/L to 50 μmol/L. This work expanded ideas for the application of pore confinement effect and provided references for the detection of disease biomarkers of gout and hyperuricemia.

Carbon dots with high luminescence intensity were synthesized. Firstly, 0.022 g of luminol and 0.015 g of L-cysteine were dispersed in 15 mL of acetic acid and sonicated uniformly. Then the precursor reacted by hydrothermal method (180 °C, 10 h) in Teflon-lined stainless steel autoclave. The solution was centrifuged constantly after cooling to room temperature naturally to remove large particles of impurities. Finally, the light yellow solution was freeze-dried to obtain a yellowish-brown powder. The remaining solids were stored in the refrigerator (4 °C). While, 1 mg CDs were dissolved in 300 mL ultrapure water (3.34 μg/mL) for further use. Next, the fabrication of sensing electrode and the detection of uric acid (UA) were as follows. Glassy carbon electrode (GCE) was polished successively in reference to the reported method [20]. Firstly, 3 μL ZIF-8 methanol solution (2 mg/mL) was dropped on the pre-processed GCE. Afterwards, 5 μL CDs solution (3.34 μg/mL) was coated on the modified GCE and dried at 25 °C (CDs/ZIF-8/GCE). The prepared ECL biosensors were tested in 2 mL 0.1 mol/L phosphate buffer saline (PBS, pH 7.4) with the working potential ranging from −0.6 V to 0.7 V (the luminescence potential and optimum scan potential of CDs are determined as shown in Fig. S1 in Supporting information), the photomultiplier tube (PMT) at 800 V and scanning rate of 0.3 V/s.

The morphologies of ZIF-8 and CDs were investigated initially by scanning electron microscopy (SEM) and transmission electron microscopy (TEM), respectively. The obtained ZIF-8 presented an ideal rhombic dodecahedral shape with uniform morphology from the SEM images (Fig. 1A). In Fig. 1B, the TEM results indicated CDs with particle diameters of about 4 nm, displaying quasi-spherical nanoparticles with even distribution. Meanwhile, visible crystalline lattice fringes with the interlayer spacing of 0.23 nm could be seen through the high-resolution TEM (HRTEM) images, corresponding well with the (1120) lattice planes of graphene [6]. In addition, the crystalline morphology of CDs was revealed by the X-Ray diffraction (XRD) images (the inset in Fig. 1C) as well. Thus, the results of both HRTEM and XRD proved that CDs possessed a partially ordered graphite carbon structure. X-ray photoelectron spectroscopy (XPS) and Fourier transform infrared (FT-IR) spectra were employed subsequently to examine the surface functional groups of CDs. The obvious characteristic peaks of S 2p, N 1s and O 1s

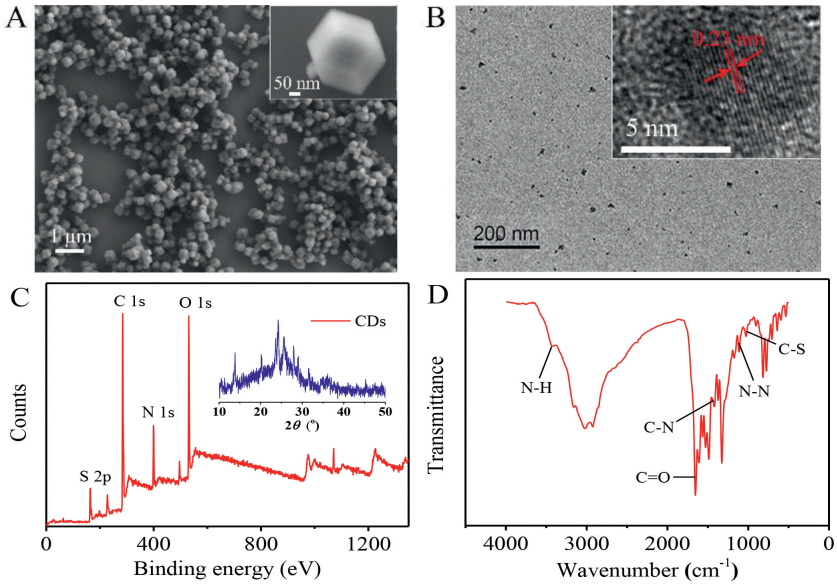

Fig. 1. (A) ZIF-8 SEM image. (B) CDs TEM image (inset: the crystalline morphology of CDs). (C) CDs XPS spectrum for full region (inset: the XRD pattern of CDs). (D) CDs FT-IR spectrum from 500 cm^{-1} to 4000 cm^{-1}.

could be observed clearly from the XPS maps (Fig. 1C), which illustrated that the presences of N, S elements in the structure of CDs. It was inferred preliminarily that N, S elements had been doped into the graphite carbon structure of CDs successfully. As shown in Fig. 1D, strong absorption bands peaked at 3431 cm^{-1} and 1653 cm^{-1} were observed, which were attributed to the N–H and C=O stretching vibrations of the amide bond, respectively [5]. The characteristic absorption peak occurring at 1113 cm^{-1} was assigned to the N–N stretching vibration. This elucidated strongly that there were abundant hydrazide groups on the surface of CDs, which might be originated from the luminol. At the same time, there were obvious characteristic peaks at 1420 cm^{-1} and 1026 cm^{-1} which were assigned to the stretching vibration peaks of C–N and C–S (that was consistent with XPS maps in Fig. 1C), respectively. In conclusion, these results traced out the structure of CDs, which was composed of N, S doping partially ordered graphite carbon structure and possessed the hydrazine functional groups.

UV-vis, photoluminescence (PL) and ECL spectra were obtained to provide the evidence of optical characterization of CDs, respectively. The UV-vis absorption spectrum of CDs exhibited a distinct peak at 220 nm, as shown in Fig. 2A, which was assigned to a typical π-π^* transition [5], proving convincingly the carbon graphite structure of CDs again. The absorption peaks at 283, 320 and 340 nm belonged to n-π^* transition due to the conjugation of carbon graphite and hydrazine. From the inset in Fig. 2B, CDs presented light yellow and bright blue photoluminescence under the visible light and UV light (365 nm), respectively. The PL spectra (Fig. 2B) revealed that CDs were excited at 364 nm (black line) and emitted photoluminescence at 429 nm (red line). A maximum ECL emission peak locating at 433 nm of CDs/GCE was obtained by the three-

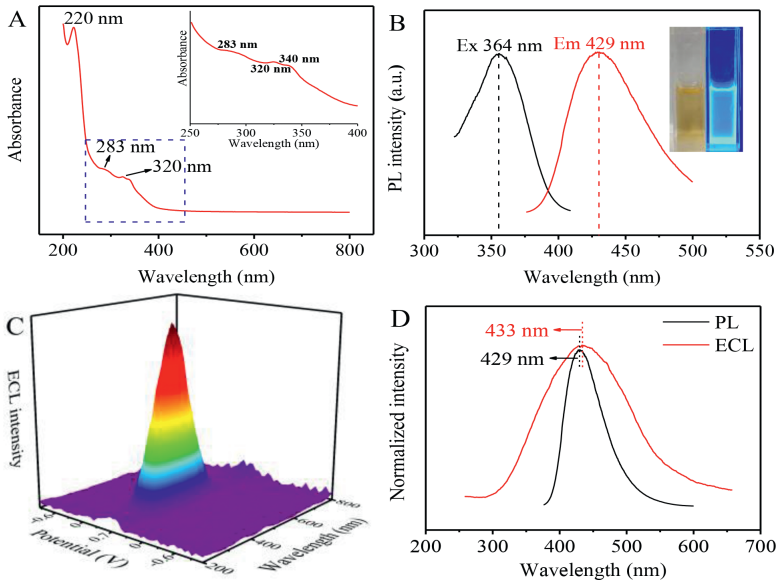

Fig. 2. Characterization of CDs with (A) UV-vis absorbance (the inset corresponding to the local magnification UV-vis absorbance) and (B) PL spectra (Ex, black line, Em, red line), the inset photograph of B is under daylight (left) and UV light (right). (C) 3D ECL image pattern and (D) normalized PL spectrum (black line) and 2D ECL spectrum (red line).

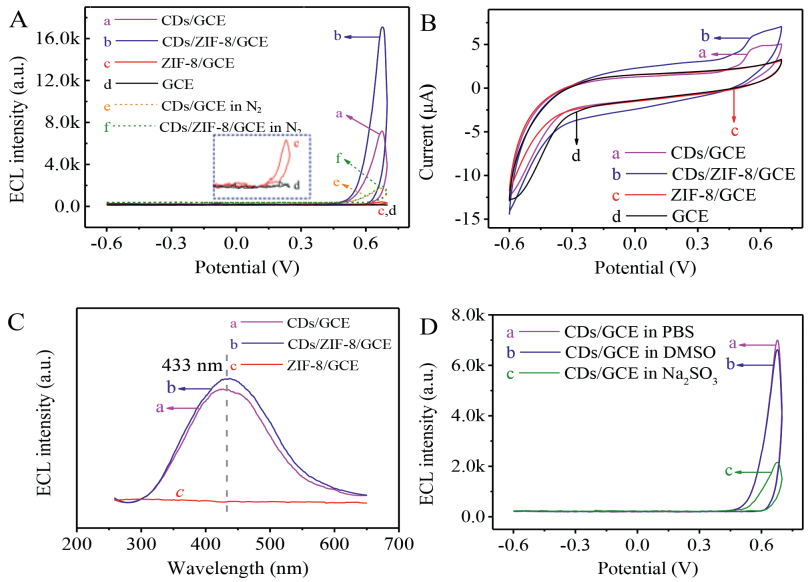

Fig. 3. (A) ECL-potential curves of (a) CDs/GCE, (b) CDs/ZIF-8/GCE, (c) ZIF-8/GCE, (d) GCE in PBS, (e) CDs/GCE, (f) CDs/ZIF-8/GCE in N_2-saturated PBS. (B) CV curves of (a) CDs/GCE, (b) CDs/ZIF-8/GCE, (c) ZIF-8/GCE, (d) GCE in PBS. (C) 2D ECL spectra of (a) CDs/GCE, (b) CDs/ZIF-8/GCE, (c) ZIF-8/GCE in PBS. (D) ECL-potential curves of CDs/GCE in 0.1 mol/L PBS (a), 0.1 mol/L PBS containing 10 mmol/L DMSO (b) and 0.1 mol/L PBS containing 10 mmol/L Na_2SO_3 (c), respectively. All ECL and CV scanning voltage was −0.6~0.7 V.

dimensional (3D) color map surface (Fig. 2C). As displayed in Fig. 2D, the maximum ECL peak of CDs (red line) was similar relative to its PL spectrum (black line, 429 nm), indicating that the ECL of CDs originated from eigenstate luminescence.

ECL, cyclic voltammetry (CV) and 2D ECL spectra were carried out to explore the mechanism of the ZIF-8/CDs modified GCE. As could be seen from Fig. 3A, the ECL signal (7000 a.u.) of CDs/GCE (curve a) was observed clearly in the presence of endogenous coreactant. CDs/ZIF-8/GCE (curve b) increased anodic ECL signal (17300 a.u.) up to 250% obviously at the same concentration of CDs, which proved effectively that ZIF-8 promoted the luminescence of CDs. Meanwhile, the anodic peak current of CDs/ZIF-8/GCE at about 0.6 V was prominently enhanced than that of CDs/GCE (as shown in Fig. 3B, curves a and b), indicating that more CDs had participated in the process of oxidation reaction. By contrast, a negligible response signal (about 200 a.u.) was produced by both ZIF-8/GCE and bare GCE in Fig. 3A (curves c and d), demonstrating that the ECL emitters were CDs. It corresponded to CV curves of c and d in Fig. 3B, whose oxidation peak disappeared. In the meantime, CDs/ZIF-8/GCE had the same emission wavelength (curve b) of 433 nm as that of CDs/GCE (curve a) from ECL characteristic spectra in Fig. 3C. While the ZIF-8/GCE had no ECL response peak at 433 nm (curve c in Fig. 3C), indicating that the ECL originated from the CDs rather than ZIF-8.

Furthermore, compared with curves a and b in Fig. 3A, both CDs/ZIF-8/GCE and CDs/GCE had a weak response in N_2-saturated PBS (Fig. 3A, curves e and f), thus confirming dissolved O_2 performed as a coreactant. It has been reported that dissolved O_2,

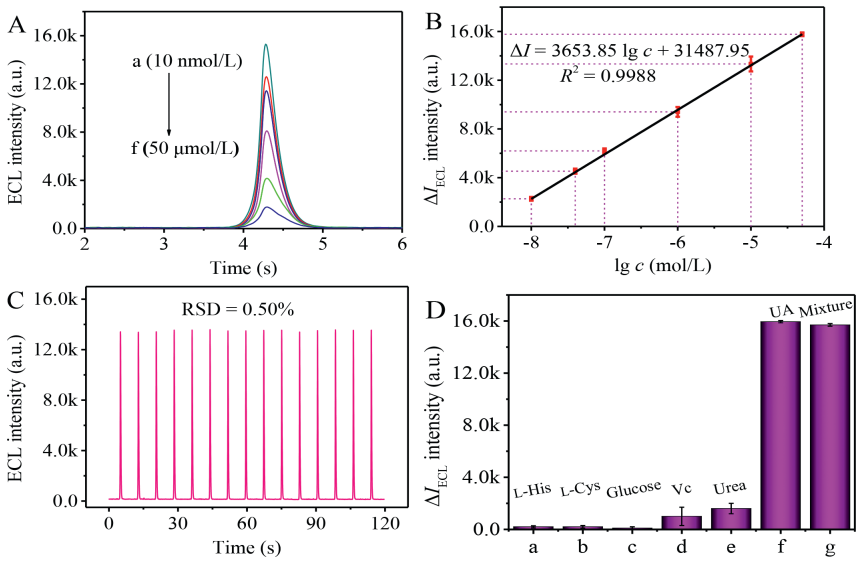

Fig. 4. (A) ECL response signals of the prepared biosensor to different concentrations of UA from 10 nmol/L to 50 μmol/L (a-f). (B) Corresponding calibration curve for the UA determination. (C) Stability of CDs/ZIF-8/GCE containing 50 nmol/L UA in PBS (pH 7.4). (D) Selectivity of UA biosensor, the concentration of the above interference agents at 5 mmol/L, including L-arginine (L-His), L-cysteine (L-Cys), glucose, L-ascorbic acid (Vc), urea and 50 μmol/L of UA. ECL responses were all measured with potential of −0.6~0.7 V in 0.1 mol/L PBS (pH 7.4), scan rate of 0.3 V/s, PMT biased 800 V and magnitude 4.

as endogenous coreactant, generates a variety of ROSs ($O_2{}^1$, $^{\bullet}OH$ and $O_2{}^{\bullet-}$) to react with the active intermediates of luminophor [15]. Consequently, different capture agents (DMSO absorb $^{\bullet}OH$ and Na_2SO_3 assimilate $O_2{}^{\bullet-}$, respectively) were added to the PBS to further explore the process of ROSs participating directly in ECL emission in Fig. 3D. The ECL response was similar (curve b) with CDs/GCE in PBS (curve a) when DMSO was added to PBS, demonstrating that $^{\bullet}OH$ was not closely related to ECL reaction. It could be seen from curve c that the signal was reduced obviously in the existence of Na_2SO_3. Consequently, $O_2{}^{\bullet-}$ was presumed to be involved directly in ECL emission (specific reaction mechanism could be seen from Scheme 1C).

It is of great significance to design the accurate and sensitive uric acid (UA) detection method since the abnormal UA usually leads to gout and higher blood UA disease [21]. As shown in Fig. 4A, the ECL signal decreased when the UA concentration increased within the scope of 10 nmol/L to 50 μmol/L because ROSs could be quenched by UA effectively (a-f). It was worth noting that the changes of ECL response (Fig. 4B) with the logarithm of UA concentration exhibited an outstanding linear relationship fitted as $\Delta I = 3653.85 \lg c + 31487.95$ ($R^2 = 0.9988$). According to the 3σ rule [22], the detection limit was 3.52 nmol/L of the UA biosensor. To explore the stability of biosensor (Fig. 4C), the ECL response signal was measured by continuous scanning for 15 cycles of CDs/ZIF-8/GCE in PBS (pH 7.4) containing 50 nmol/L UA. The relative standard deviation (RSD) was calculated as low as 0.50%, attesting that UA biosensor had an excellent stability. Additionally, to evaluate the specificity of the UA biosensor, small organic molecules in serum as potential interference substances were investigated under the same experimental conditions, including L-arginine (L-His), L-cysteine (L-Cys), glucose, L-ascorbic acid (Vc) and urea. When the concentrations of the above interference agents were increased to 100-fold (5 mmol/L) as compared with UA (50 μmol/L), the ECL responses (Fig. 4D) generated by the interference agents were obviously lower than that of UA, indicating that the constructed UA sensing platform displayed a favorable selectivity.

In summary, an efficient and concise exogenous coreactant-free ECL system based on CDs assembled ZIF-8 had been constructed skillfully through the combination of pre-placement strategy to CDs and "pore confinement-enhanced ECL" effect. N, S doped CDs with low excitation potential and high ECL intensity contained abundant hydrazide groups. Impressively, the prepared ZIF-8 played two following crucial roles in this work. On the one hand, ZIF-8 serving as a matrix for CDs increased the immobilization and stability of CDs. The uniform distribution of CDs on the surface of ZIF-8 shortened the electron and proton transport distance between CDs and dissolved O_2. On the other hand, ZIF-8 could preconcentrate dissolved O_2 through the porous structure and promote the productivity of ROSs in framework for the existence of abundant pyridine nitrogen. The reaction efficiency of CDs with dissolved O_2 increased due to the effect of pore confinement-enhanced ECL. This work expanded ideas for the application of pore confinement effect and provided references for the detection of disease biomarkers of gout and hyperuricemia.

Declaration of competing interest

The authors declare that they have no known competing financial interests or personal relationships that could have appeared to influence the work reported in this paper.

Acknowledgments

This work was financially supported by the NNSF of China (No. 22022408), the Chongqing Talents Personnel Support Program (No. CQYC201905067) and the Fundamental Research Funds for the Central Universities (No. XDJK2019TJ002).

Supplementary materials

Supplementary material associated with this article can be found, in the online version, at doi:10.1016/j.cclet.2022.01.010.

References

[1] H. Liu, Y. Sun, Z. Li, et al., Chin. Chem. Lett. 30 (2019) 1647–1651.
[2] W. Lv, X. Wang, J. Wu, H. Li, F. Li, Chin. Chem. Lett. 30 (2019) 1635–1638.
[3] K. Jiang, S. Sun, L. Zhang, et al., Angew. Chem. Int. Ed. 54 (2015) 5360–5363.
[4] N.A. Travlou, J. Secor, T.J. Bandosz, Carbon 114 (2017) 544–556.
[5] A. Chen, W. Liang, H. Wang, et al., Anal. Chem. 92 (2020) 1379–1385.
[6] R. Zhang, J.R. Adsetts, Y. Nie, X. Sun, Z. Ding, Carbon 129 (2018) 45–53.
[7] J. Chen, J. Yan, Q. Feng, et al., Biosens. Bioelectron. 176 (2021) 112955.
[8] D. Li, P. Jing, L. Sun, et al., Adv. Mater. 30 (2018) 1705913.
[9] C.V. Raju, G. Kalaiyarasan, S. Paramasivam, J. Joseph, S.S. Kumar, Electrochim. Acta 331 (2020) 135391.
[10] F. Arcudi, L. Ethordevic, S. Rebeccani, et al., Adv. Sci. 8 (2021) 2100125.
[11] Y.M. Lei, Y. Zhuo, M.L. Guo, Y.Q. Chai, R. Yuan, Anal. Chem. 92 (2020) 2839–2846.
[12] Y. He, J. Du, J. Luo, S. Chen, R. Yuan, Biosens. Bioelectron. 150 (2020) 111898.
[13] T.Watanabe Irkham, A. Fiorani, et al., J. Am. Chem. Soc. 138 (2016) 15636–15641.
[14] H. Zhang, X. Zhang, S. Dong, Anal. Chem. 87 (2015) 11167–11170.
[15] L. Wang, M.H. Jiang, Y.Q. Chai, R. Yuan, Y. Zhuo, Chem. Commun. 56 (2020) 9000–9003.
[16] W.J. Zeng, K. Wang, W.B. Liang, et al., Chem. Sci. 11 (2020) 5410–5414.
[17] J. Chen, H. Gao, Z. Li, Y. Li, Q. Yuan, Chin. Chem. Lett. 31 (2020) 1398–1401.
[18] N. Liao, X. Zhong, W.B. Liang, R. Yuan, Y. Zhuo, Acta Chim. Sin. 79 (2021) 1257–1264.
[19] W. Xue, Q. Zhou, F. Li, B.S. Ondon, J. Power Sources 423 (2019) 9–17.
[20] M.C. Pan, Y.M. Lei, Y.Q. Chai, R. Yuan, Y. Zhuo, Anal. Chem. 92 (2020) 13581–13587.
[21] N. Liao, J.Y. Zhang, Z.Y. Huang, et al., Chem. J. Chin. Univ. 41 (2020) 1989–1995.
[22] W.J. Zeng, N. Liao, Y.M. Lei, et al., Biosens. Bioelectron. 100 (2018) 490–496.